



Assessment of accuracy of the structure-factor-size-estimator method in determining red blood cell aggregate size from ultrasound spectrum backscattering coefficient

**Ratan K Saha<sup>1</sup>, Emilie Franceschini<sup>2</sup> and Guy Cloutier<sup>3,4</sup>**

<sup>1</sup>Department of Physics, Ryerson University, 350 Victoria Street, Toronto, Ontario, M5B 2K3, Canada.

<sup>2</sup>Laboratoire de Mécanique d'Acoustique LMA - CNRS UPR 7051, 31 Chemin Joseph Aiguier, 13402 Marseille, Cedex 20, France.

<sup>3</sup>Laboratory of Biorheology and Medical Ultrasonics, University of Montreal Hospital Research Centre (CRCHUM), 2099 Alexandre de Sève (Room Y-1619), Montreal, Quebec H2L 2W5, Canada.

<sup>4</sup>Department of Radiology, Radio-Oncology and Nuclear Medicine, and Institute of Biomedical Engineering, University of Montreal, Montreal, Quebec, Canada.

Running title: Erythrocyte aggregate size estimation.

Key words: Hexagonal close packing of erythrocytes, red blood cell cluster size determination, RBC aggregation, ultrasound tissue characterization, quantitative ultrasound.

## Abstract

A computer simulation algorithm suitable for generating non-overlapping, isotropic and fairly identical red blood cell (RBC) clusters is presented. RBCs were stacked following the hexagonal close packing (HCP) structure to form a compact spherical aggregate. Such an aggregate was repeated and placed randomly under non-overlapping condition in three-dimensional space to mimic an aggregated blood sample. Backscattering coefficients (BSCs) were computed for samples at various cluster sizes and different hematocrits showing BSC increases with mean aggregate sizes. The accuracy of the structure factor size estimator (SFSE) method in determining mean aggregate size and packing factor were also examined. A good correlation ( $R^2 \geq 0.94$ ) between the mean size of aggregates predicted by the SFSE and true size was found for each hematocrit. This study shows that for spherical aggregates there exists a region for each hematocrit where SFSE works most accurately. Typically, error of SFSE in estimating mean cluster size was  $< 20\%$  for dimensions between 14-17  $\mu\text{m}$  at 40% hematocrit. This study suggests that the theoretical framework of SFSE is valid under the assumption of isotropic aggregates.

PACS Number(s): 43.20.Fn, 43.30.Ft, 43.80 Cs, 87.10 Rt.

## 1. Introduction:

Ultrasonic tissue characterization techniques generally (sometimes the signal envelope statistics is used [1]) consider frequency dependent information of backscatter echoes to quantify tissue structural properties such as the size, acoustic impedance, number density of scattering particles, etc. This approach has been successfully used for the characterization of the eye [2], [3], liver [4], kidney [5], prostate [6], breast tissues [7] and also to monitor cell apoptosis in order to evaluate efficacy of cancer therapies [8]. The blood tissue has also been characterized by employing this technique [9]. The main purpose of ultrasonic characterization of blood is to assess the level of red blood cell aggregation, which is a surrogate marker of inflammation [10]. An enhanced level of RBC aggregation is a pathological state and is associated with many circulatory diseases such as deep venous thrombosis, atherosclerosis and diabetes mellitus. The ultrasonic backscattering technique has the potential to provide a method for non-invasive determination of RBC cluster size, consequently allowing addressing the role of RBC aggregation in the processes of such diseases.

Yu and Cloutier [11] recently proposed a parametric form of backscattering coefficient. They arrived at that mathematical form by using a second order Taylor series expansion of the structure factor and thus obtained two physically relevant parameters of aggregation, the mean diameter of aggregates  $D$  and the packing factor  $W$ . The packing factor is related with the volume ratio of RBCs known as the hematocrit ( $H$ ), and is sensitive to the spatial arrangement of scatterers. The other parameter  $D$  estimates how many cells are attached as an aggregate. They used the parametric form of the backscattering coefficient to analyze experimental data *in vitro* and obtained sound rheological results [12]. The method is referred as the structure factor size estimator (SFSE). Franceschini et al. [13] further developed this model to incorporate attenuation

effect of intervening tissues between the probe and the blood flow with the objective of providing a method applicable to *in vivo* situations. It was shown in that work that simultaneous evaluation of  $D$ ,  $W$  and of the attenuation coefficient of the intervening tissue layers could be obtained. However, the experimental assessment of accuracy of SFSE in determining mean size of aggregates by optical means was possible only at a low hematocrit (6%), since RBCs are not visible with a microscope at a normal physiological hematocrit of typically 35% to 55% [11].

The aim of the work presented here is to describe a simple and rapid method to simulate randomly distributed compact RBC clusters in order to evaluate the accuracy of the SFSE method. The cells were assumed to arrange in a spherical cluster in such a way so that a hexagonal close packing (HCP) structure was obtained. Note that this scheme provides the highest packing density (i.e. fractional volume occupied by spheres and also referred as the hematocrit ( $H$ )) that is about 0.74 for spheres [14]. Such an aggregate was repeated and placed randomly under non-overlapping condition in the three dimensional space to mimic aggregated blood samples. The ensemble average of the backscattering coefficient was determined by simulation from the samples comprising non-overlapping, isotropic and fairly identical spherical RBC aggregates. Consequently, cluster size dependent ultrasound backscattering properties were studied. The accuracy of the SFSE method in estimating mean cluster size was also assessed by comparing results with simulated cluster sizes at hematocrits from 0.20 to 0.40, which is not possible experimentally by optical means. A low hematocrit of 0.20 is a condition that can be encountered in severe anemia. The approach described here as far as our knowledge has never been employed to generate RBC aggregates as well as to study ultrasound backscattering from a collection of such aggregates.

The paper is organized in the following way. In section 2 we discuss the theoretical models describing ultrasonic backscattering by a collection of erythrocytes. Section 3 illustrates the simulation method. Results are presented in section 4. Quality of our results in the light of experimental observations is discussed in section 5 followed by a summary in section 6.

## 2. Theoretical model:

The backscattering cross-section per unit volume or the backscattering coefficient for the scattering of an incident plane wave with wave vector  $\vec{k}$  by an ensemble of particles of uniform size can be cast in terms of the Percus-Yevick packing factor ( $W_{PY}$ ) as in [9]:

$$\chi_b(-2\vec{k}) = mW_{PY}\sigma_b(-2\vec{k}), \quad (1)$$

where,  $m$  is the number density of particles and it is related with the hematocrit ( $H$ ) as  $m = H/V_s$ . Here,  $V_s$  denotes the volume of an equivalent sphere of a RBC, which is a good model of the backscattering cross-section  $\sigma_b(-2\vec{k})$  (less than 5% error) below 21 MHz [15]. The subscript  $b$  here indicates backscattering. The Percus-Yevick packing factor ( $W_{PY}$ ) for hard spherical particles can be expressed as [9]:

$$W_{PY} = \frac{(1-H)^4}{(1+2H)^2} \quad (2)$$

The analytical expression of the backscattering cross-section for the scattering of an incident plane wave by a weak spherical scatterer of radius  $a$  can be derived by using the Born approximation and it is given by [16]:

$$\sigma_b(-2\vec{k}) = \frac{1}{16\pi^2} V_s^2 k^4 \left( \frac{\kappa_e - \kappa}{\kappa} - \frac{\rho_e - \rho}{\rho_e} \right)^2 \left( 3 \frac{\sin 2ka - 2ka \cos 2ka}{(2ka)^3} \right)^2 \quad (3)$$

Here,  $\kappa$  and  $\rho$  indicate the adiabatic compressibility and density of the surrounding medium (blood plasma), respectively. The same quantities for the RBC scatterer are given by  $\kappa_e$  and  $\rho_e$ . Eq. (1) is valid in the low frequency range and observed to provide good fit to experimental data for the backscattering of non-aggregated RBCs when probed at 7.5 MHz [17].

On the other hand, the resultant backscatter signal from a collection of particles can be obtained by using the linear superposition principle for signals backscattered by individual particles. Corresponding backscattering coefficient for particles with equal radii can be written as [18], [19]:

$$\chi_b(-2\vec{k}) = m \left\langle \frac{1}{N} \left| \sum_{n=1}^N \exp(i2\vec{k} \cdot \vec{r}_n) \right|^2 \right\rangle \sigma_b(-2\vec{k}) = mS(-2\vec{k})\sigma_b(-2\vec{k}) \quad (4)$$

where,  $S(-2\vec{k})$  is the structure factor of the medium and dictates how backscattering would vary with spatial organization of particles. The symbol  $\langle \rangle$  states for ensemble average. The position vector  $\vec{r}_n$  defines the center of the  $n^{\text{th}}$  spherical scatterer in space and  $N$  is the total number of scatterers in the region of interest. In general, the structure factor of a medium containing particles distributed in the three dimensional (3D) space can be determined from the 3D Fourier transform of the spatial distribution of particles [18]. However, if the direction of the interrogating wave coincides with an axis of the coordinate system of the region of interest (ROI), then Eq. (4) reduces to one dimensional form and therefore computation of structure factor becomes trivial. In this work, Eq. (4) was computed for samples composed of randomly distributed 3D RBC clusters, which were isotropic and fairly similar in size. Accordingly cluster size dependent backscattering was examined.

Recently, Yu and Cloutier [11] used a second order Taylor series expansion of the structure factor to obtain two physically relevant parameters, namely  $W$  and  $D$ . The parameter  $D$  was computed from the mean radius of gyration ( $R_g$ ) of the aggregates. With this expansion Eq. (4) reduces to:

$$\chi_b(-2\vec{k}) = m(W - 4k^2 R_g^2) \sigma_b(-2\vec{k}) \quad (5)$$

The radius ( $R_{sp}$ ) of a homogeneous spherical object is related to its radius of gyration as  $R_{sp} = \sqrt{5/3} R_g$  and thus mean size of aggregates in terms of number of RBCs could be presented as,  $D = R_{sp} / a$ . Yu and Cloutier used Eq. (5) to fit measured backscattering data corresponding to different RBC aggregation levels and the technique was referred as the structure factor size estimator (SFSE) method. In the present study, we also employed Eq. (5) to fit simulated frequency dependent backscattering coefficient curves obtained by computing Eq. (4) for different samples with various clustering conditions. This enabled us to examine cluster size dependent ultrasound backscattering by RBCs as well as to assess the SFSE method by comparing mean cluster size from simulated aggregates to that predicted by the said method from simulated backscattering coefficient.

### 3. Simulation method:

#### 3.1 Simulation of spatial distributions of aggregated RBCs:

Different approaches to simulate compact RBC aggregates have been explored. For example, RBC clusters could be generated by allowing particles to interact via a Morse type potential and then by evolving the system through random throwing of cells [18]. However, this technique is computationally intensive and can only produce random loose packing (RLP)

configurations of particles with packing fractions of  $0.60 \pm 0.02$  in three dimensions [20]. Moreover, previously only 5.5 dB enhancement of BSC was found at 7.5 MHz at the highest aggregating condition at  $H = 0.40$  using this technique [18] and that is on the lower side compared to experimentally measured values. Alternatively, one can rely on algorithms to construct random close packing (RCP) configurations [21], [22] that are expected to increase BSC. Jodrey and Tory [22] developed this algorithm to generate RCP of equal spheres from a random distribution of points. In that study, each point is the center of an inner and an outer sphere. RCP configuration was achieved by slowly shrinking the outer diameter and by eliminating overlapping of outer spheres. The procedure terminated when two diameters became on the same order. The implementation of such RCP algorithms is not straightforward, they are computationally intensive and also the attainable packing fraction ( $0.64 \pm 0.02$ ) of particles is still limited.

On the other hand, a highest packing density (0.74) can be obtained by using regular packing schemes such as hexagonal close packing (HCP) or cubic close packing (CCP) [14]. As mentioned earlier, it is expected that significant enhancement of BSC would be possible by using hexagonal close packing of cells. In the current study, we followed this scheme to form an aggregate. The generation of such structure is simple and fast because cells have to be placed only at some defined locations. Such an aggregate prototype could be repeated and placed randomly in the three dimensional space to generate a tissue realization consisting of non-overlapping, isotropic and fairly identical RBC clusters.

Initially, spatial locations of centers of clusters of identical size were chosen randomly within the region of interest (ROI) under the condition that they would not overlap. The periodic boundary conditions were imposed during this process. That means the clusters at the boundaries

of the ROI would not overlap with the others at the opposite boundaries and thus removed the edge effect. The total number (fixed by the size of the ROI and the hematocrit) of cells was equally divided (truncated to the nearest lower integer value) into these clusters and the cells stacked by following hexagonal close packing structure for each cluster.

To accomplish this (see Fig. 1), at the beginning a large number (arbitrarily chosen) of spheres representing RBCs were packed within a box. They were stacked in such a way that they formed a HCP structure [14]. After that, the coordinates of the centers of spheres with respect to the center of a sphere located at the central region of the box were recorded according to their distances and stored in a lookup table. The next step was to take the coordinates of the required number of RBC mimicking spheres from the lookup table. Accordingly, spheres were stacked with respect to the center of a cluster and thus the HCP structure was obtained. This step was repeated for each cluster. The position coordinates with respect to the ROI of a sphere belonging to a cluster were determined by summing its coordinates available from the lookup table and the coordinates of the center of that cluster. Thus, the coordinates obtained from the lookup table were transformed into the coordinate system of the ROI. The position coordinates with respect to the ROI of the cells belonging to the other clusters were also obtained. The remaining spheres (those did not belong to any cluster and would behave as disaggregated RBCs) were thrown randomly in the ROI maintaining non-overlapping condition under periodic boundary conditions with the existing spheres. Further, an additional step was conducted to find overlapping pairs of cells. If found then a new coordinate under non-overlapping condition was assigned for one of them. In this case too periodic boundary conditions were imposed while checking the non-overlapping condition of that cell with the others. In this way, spatial organization of spheres

(most of them were included within clusters and others were randomly distributed in the ROI) mimicking a tissue sample was obtained.

The radius of gyration of a cluster of that tissue sample was computed by using the distances of the constituent spheres with respect to the center of the cluster. This was done for each cluster and accordingly the mean radius of gyration of clusters was obtained. The mean size of clusters ( $R_{sim}$ ) was then determined by multiplying the average radius of gyration with the factor  $\sqrt{5/3}$ , as described above. Note that the non-aggregated RBCs were not taken into account during this estimation. Fig. 1 summarizes this procedure through a flow chart diagram. The computed numerical value of ( $R_{sim}$ ) acted as a gold standard and further used to assess accuracy of the SFSE.

### 3.2 Computation of a simulated BSC curve:

The size of the ROI was fixed to  $1000 \times 125 \times 125 \mu\text{m}^3$ . The backscattering measurements were carried out for the scattering of incident plane waves propagating along the longest dimension of the ROI and that was considered as the  $x$  axis in this case. The length of the ROI along the  $x$  axis was sufficiently large and therefore provided good resolution in the frequency domain. However, much smaller dimensions were used along the two other lateral directions. This was done to restrict the volume of the ROI, the number of RBCs and the computational time. The number of particles for this size of ROI was 35919, 53879 and 71839 at 20%, 30% and 40% hematocrits, respectively. The radius of the equivalent sphere of a RBC was  $2.75 \mu\text{m}$ , corresponding to a typical RBC volume of  $87 \mu\text{m}^3$ . The numerical values of density and compressibility of a RBC were assigned as  $\rho_e = 1.092 \text{ g/cm}^3$  and  $\kappa_e = 34.1 \times 10^{-12} \text{ cm}^2/\text{dyne}$ , respectively. The same quantities for the ambient medium (plasma) were chosen as  $\rho = 1.005$

$\text{g/cm}^3$  and  $\kappa = 44.3 \times 10^{-12} \text{ cm}^2/\text{dyne}$ , respectively [17]. For each sample, the cluster size frequency dependent backscattering coefficient was obtained by evaluating Eq. (4) and a mean curve was determined from 250 different tissue realizations.

### 3.3 Fitting of a simulated mean BSC curve with the SFSE:

The final step was to fit the simulated mean BSC curve with the SFSE between 5 MHz and the frequency corresponding to the first minimum of that curve on a log-log scale. It may be noted that depending upon the cluster size, the mean BSC curve exhibited minima at some frequencies. The parameters  $W$  and  $R_{sp}$  were obtained by optimizing Eq. (5) and the simulated BSC curve. The optimization was carried out by using the “fminsearch” function of Matlab 7.8.0.347 (R2009a). The mean size of aggregates ( $R_{sp}$ ) and average simulated size ( $R_{sim}$ ) were then compared to examine the accuracy of the SFSE method. This procedure was carried out at three hematocrit levels for different cluster sizes.

## 4. Results:

Figure 2(a) presents an arrangement of 51 spheres or RBCs in hexagonal close packing forming a spherical 3D cluster. A realization of an aggregated blood tissue is shown in Fig. 2(b). As an example and for clarity of the figure, a smaller ROI ( $200 \times 20 \times 20 \mu\text{m}^3$ ) occupied by the RBCs at 14% hematocrit is displayed. However, BSC curves shown in later sections were computed for a ROI of  $1000 \times 125 \times 125 \mu\text{m}^3$ . Figure 2(b) contains four non-overlapping, identical, randomly placed RBC clusters and each cluster is composed of 51 RBCs. These clusters maintained periodic boundary conditions. That means if a portion of a cluster crossed a boundary wall then that portion appeared at the opposite side.

Figure 3(a)-(c) demonstrate variations of the backscattering coefficient at some clustering conditions for three hematocrits over a large frequency range (750 KHz - 200 MHz, computed using Eq. (4)). The simulated clusters were tightly packed by the cells leaving small number of cells as non-aggregated cells. For example, for a sample simulated realization at 0.20 hematocrit ( $R_{sim} = 9.60 \pm 0.06 \mu\text{m}$  in Fig. 3(a)), 98.37% RBCs of the total number of cells formed aggregates and remaining 1.63% cells were distributed randomly in space. In another case at 0.40 hematocrit ( $R_{sim} = 17.11 \pm 0.32 \mu\text{m}$ , Fig. 3(c)) these numbers were 92.28% and 7.72%, respectively. The mean radius of simulated three dimensional isotropic clusters is presented in the legend denoting the corresponding aggregation level for each sample. BSC predicted by the Percus-Yevick packing theory is also shown for comparison. The Percus-Yevick theory describes backscattering properties of non-aggregated RBCs in the low frequency regime (1-30 MHz typically), where  $ka < \pi / 10$  [9]. It may also be noticed from Fig. 3 that BSC between 750 KHz to the frequency corresponding to the first maximum increased as the cluster size increased for all samples. Moreover, the first minimum (or the first maximum) appeared at a lower frequency for a sample containing aggregates than that of the non-aggregated blood. For example, the first minimum in Fig. 3(a) occurred at about 195 MHz for the Percus-Yevick curve but it appeared nearly 60 MHz for the first sample with simulated mean aggregate sizes of  $R_{sim} = 9.60 \pm 0.06 \mu\text{m}$ . Note that the position of the first minimum is a signature of the size of the scattering objects (either individual cells or clumps composed of collection of cells) [23]. For any hematocrits, the first minimum appeared at lower frequencies as bigger aggregates were simulated.

Figure 3(d) illustrates how the backscattering coefficient measured at 7.5 MHz (normalized by that of the Percus-Yevick theory and expressed in dB) varies with cluster size. It

is evident from the figure that BSC increased as the mean size of clusters increased [24] and it is true for all hematocrits. Further, the relative increase of BSC with respect to that of the Percus-Yevick packing theory for a particular cluster size is always higher at  $H = 0.30$  than that of  $H = 0.20$ . For instance, at  $R_{sim} \approx 12.0 \mu\text{m}$  the relative increase of BSC is about 12 dB for  $H = 0.20$  but it is nearly 14 dB at  $H = 0.30$ . However for  $H = 0.40$ , the relative increase is less than those at the other hematocrits for the smaller cluster size but reaches close to that of  $H = 0.30$  for the larger cluster size considered in this study. Additionally, although we did not present it graphically, we observed that spectral slopes on a log-log scale between 1 to 10 MHz remained around 4 (Rayleigh scattering regime) for all samples at all three hematocrits.

Figure 4(a) displays simulated frequency dependent BSC curves fitted with the structure factor size estimator method for the same clustering conditions described in Fig. 3(a). The estimated values of  $R_{sp}$  and  $W$  are presented in the legend. It is clear from the figure that the second order expansion of the structure factor is insufficient to model the complex behavior of BSC. Indeed, some disagreements between simulated and fitted SFSE curves are present, especially in the low frequency range, where each fitted curve over-estimates the backscattering coefficient. Figure 4(b) and (c) demonstrate fittings of BSC curves with SFSE, for  $H = 0.30$  and  $0.40$ , respectively. Fitting characteristics are similar to that of (a).

To assess the accuracy of the SFSE method, we have plotted (see Fig. 5(a)) the estimated values of  $R_{sp}$  as a function of  $R_{sim}$  for all three hematocrits. The linear regression lines are also shown in the figure. Although the SFSE model did not provide good fittings to the simulated BSCs, still excellent correlations ( $R^2 \geq 0.94$ ) were found between estimated and true cluster sizes for each hematocrit. Furthermore, it can be seen that for each hematocrit there is a region where the SFSE method works at its best. For example, error associated with the prediction of the

structure factor size estimator method is less than 20% when the mean size of aggregates varies between 14 to 17  $\mu\text{m}$  at 40% hematocrit. However, below this range SFSE under-estimates the aggregate size but above this range it over-estimates the size, especially at the lower hematocrits. The variation of  $W$  with square of  $R_{sim}$  is shown in Fig. 5(b) for all hematocrits. It is evident that  $W$  and  $R_{sim}$  follow a quadratic relationship. Straight line fits were also obtained by using the least square fitting technique and good correlations ( $R^2 \geq 0.92$ ) were found between  $W$  and  $R_{sim}^2$  for each hematocrit.

## 5. Discussions:

The scheme discussed in this paper is based on a phenomenological approach to simulate RBC clusters. It did not consider realistic interactions between the cells. It is a simple method because cells within a cluster stacked in a particular way to form the hexagonal close packing structure and provided tightly packed aggregates. This is also a fast method to generate tissue realizations mimicking aggregated red blood cell samples because RBCs can only be located at defined positions. For example, at 40% hematocrit it took about 42 seconds in a remote computer cluster to generate a tissue configuration consisting of aggregates with a mean radius of  $17.11 \pm 0.32 \mu\text{m}$ . Similarly, for another sample (with a mean aggregate radius of  $12.59 \pm 0.29 \mu\text{m}$ ) at that hematocrit, approximately 72 seconds was required to generate each configuration with the same computing platform. In this case the number of clusters was higher because it contained smaller aggregates than the previous one. Thus, the execution time was slightly more since it was needed to assign coordinates for more number of cluster centers at non-overlapping condition.

In this study, we found that BSC increased as the cluster size increased. For instance, nearly 17 dB enhancement of BSC at  $H = 0.40$  was measured at 7.5 MHz frequency for the

biggest cluster size (with mean radius of  $17.11 \pm 0.32 \mu\text{m}$ ) with respect to that of non-aggregating blood (see Fig. 3(d)). This observation is in accordance with previous experimental works. For example, Yuan and Shung [25] estimated approximately 15 dB increase of BSC at 7.5 MHz for porcine whole blood when the shear rate was decreased from 22 to  $2 \text{ s}^{-1}$ . Note that a reduction in shear rate promoted aggregation and consequently cluster size increased. The numerical values of spectral slope that we computed remained around 4 within the 1-10 MHz frequency band, where BSC curves exhibited linear variations with frequency on a log-log scale for all samples.

In addition to that, this was the first time when an attempt was made to examine the accuracy of SFSE by using simulated backscatter signals from samples containing non-overlapping, isotropic and fairly identical 3D clusters mimicking RBC aggregates. This study provided us a way to compare predicted cluster size with that of simulation. We observed excellent correlations ( $R^2 \geq 0.94$ ) between estimated and true cluster sizes for all hematocrits and also that the packing factor  $W$  maintained a quadratic relationship with the mean radius of aggregates (see Fig. 5). These findings are consistent with experimental results reported in [11]. In that work, mean sizes of RBC aggregates were determined from direct optical microscopy measurements for blood samples with 6% hematocrit at different time points of aggregation. In case of the ultrasonic method, mean sizes were estimated with the SFSE method from measured backscattered spectra at 6% hematocrit. A good correlation ( $R^2 \geq 0.76$ ) was found between optical and ultrasonic methods. As introduced earlier in this article, this comparison was not carried out at typical human hematocrits (20-55%) because it was almost impossible to get non-overlapping clusters for image processing.

The SFSE model quite satisfactorily fitted experimental BSC curves in [11] but in the present work, we did not see that much agreement between fitted curves and simulated BSC data

points (see Fig. 4). As an example we are highlighting this behavior in Fig. 6. In this figure, a simulated BSC curve (corresponding to  $R_{sim} = 17.11 \pm 0.32 \mu\text{m}$  and  $H = 0.40$ ) and the fitted SFSE curve are shown. Note that the spectral slope for the simulated curve is around 4 in the frequency band 5-13 MHz but it is about 6.5 between 13-25 MHz. This is suggesting that the SFSE method cannot take into consideration changes in spectral slope in the frequency bandwidth, where SS remains positive. It may be noted that spectral slopes superior to 4 at low frequencies could also be observed in the experiments performed by Yu and Cloutier (see Fig. 4 in [11]).

With simulations, we may have emphasized spectral slopes above 4 because we did not consider attenuation of waves, which is more important at higher frequencies. In addition to that, spectral slopes above 4 could be observed maybe because we did not consider poly-disperse clusters. In general, for poly-disperse clusters, maxima and minima locations of BSC are different for different clusters and thus a relatively smoother BSC curve can be obtained [26]. Finally, the theoretical model presented here assumes that scatterers are weak and therefore, effects of multiple scattering can be neglected. This assumption is valid for RBCs because for a red blood cell, the acoustic impedance mismatch is only about  $\approx 11\%$  with respect to the surrounding plasma.

Although we did not see good fittings of the simulated BSC curves with the SFSE but still the estimations of SFSE were good in some cluster size range. It shows that there lies a region where the structure factor size estimator method works at its best for each hematocrit. At 40% hematocrit, error associated with the prediction of SFSE in determining cluster size was within 20% when mean aggregate sizes remained within 14 to 17  $\mu\text{m}$ . Franceschini et al. [13] also mentioned in their paper that SFSE worked well for blood samples when mean radii of

clusters were  $\leq 13.90 \mu\text{m}$  for a Couette flow experiment and  $\leq 10.02 \mu\text{m}$  for a tube flow experiment. They reached to this conclusion by inspecting behaviors of correlation coefficients (BSC versus frequency of SFSE fittings). The upper limit of validity of SFSE, as found from this study, also lied in the same range but we did not observe good performance of SFSE for clusters with mean radii  $< 14 \mu\text{m}$ . One possible reason for this discrepancy is that in simulations we dealt with tightly packed clusters but in reality clusters would not be that much tight because of the presence of electrostatic repulsive potential. This potential would not allow cells to come very close to each other and thus would encourage forming loosely packed clusters, unless inflammatory related diseases are present to promote the formation of compact clusters. In other words, SFSE may work more accurately over a large range for loosely packed clusters than tightly packed clusters.

## **6. Conclusions:**

A simulation algorithm suitable for generating non-overlapping, isotropic and fairly identical RBC aggregates was presented. The red blood cells considered as homogeneous spheres were assumed to follow a hexagonal close packing structure to form compact spherical aggregates. Note that a very high packing density  $\approx 0.74$  for spheres can be achieved for this packing scheme. Such an aggregate prototype was repeated and placed randomly under non-overlapping condition in the three dimensional space to mimic aggregated blood samples. The method is simple, fast and easy to implement. The frequency dependent backscattering coefficients were computed for samples with varying mean cluster size at different hematocrits. Consequently, cluster size dependent backscattering and efficacy of the structure factor size estimator method in determining mean aggregate size were examined.

It was found that BSC increased as the mean aggregate size increased and this was true for all hematocrits. For example, at  $H = 0.40$ , BSC increased from approximately 10 to 20 dB compared to that of non-aggregated blood sample at 7.5 MHz when the mean cluster size varied from 11.5 to 17  $\mu\text{m}$ . Overall, 8 dB enhancements of BSC were observed for the other two hematocrits ( $H = 0.20$  and  $0.30$ ) from lowest to highest cluster sizes considered in this study (see Fig 3(d)), at the same interrogating frequency. Although the SFSE did not provide good fits to the simulated BSC curves but still excellent correlations ( $R^2 \geq 0.94$ ) between predicted (using the structure factor size estimator method) and true (known from simulations) mean size of aggregates were found for each hematocrit. The second estimated parameter  $W$  exhibited a quadratic relationship with mean size ( $R_{sim}$ ) of RBC aggregates for each hematocrit and in this case good correlation coefficients ( $R^2 \geq 0.92$ ) were also computed. In future, it would be interesting to incorporate real interactions between cells to form both isotropic (strong adhesive energy simulating pathological inflammatory conditions) and anisotropic (normal condition) clusters. Another interesting study might be to evaluate the performance of the Gaussian form factor model [5] to extract size information from backscatter spectra and compare that with SFSE prediction.

## 7. Acknowledgement:

This work was supported by the Canadian Institutes of Health Research (grants #MOP-84358 and CMI-72323), by the Heart and Stroke Foundation of Canada (grant #PG-05-0313), and by the National Institutes of Health of USA (grant #RO1HL078655). The authors would like to thank the “Réseau Québécois de Calcul de Haute Performance” (RQCHP), where simulations were carried out.

## 8. References:

- [1] F. Destrempes and G. Cloutier, “A critical review and uniformized representation of statistical distributions modeling the ultrasound echo envelop”, *Ultrasound Med. Biol.* **36**(7), 1037-1051, 2010.
- [2] F. L. Lizzi, M. Greenbaum, E. J. Feleppa M. Elbaum, and D. J. Coleman, “Theoretical framework for spectrum analysis in ultrasonic tissue characterization”, *J. Acoust. Soc. Am.* **73**(4), 1366-1373, 1983.
- [3] E. J. Feleppa, F. L. Lizzi, D. J. Coleman and M. M. Yaremko, “Diagnostic spectrum analysis in ophthalmology: A physical perspective”, *Ultrasound Med. Biol.* **12**(8), 623-631, 1986.
- [4] F. L. Lizzi, M. Ostromogilsky, E. J. Feleppa, M. C. Rorke and M. M. Yaremko, “Relationship of ultrasonic spectral parameters to features of tissue microstructure”, *IEEE Trans. Ultrason. Ferroelectr. Freq. Control*, **34**(3), 319-329, 1987.
- [5] M. F. Insana, R. F. Wagner, D. G. Brown and T. J. Hall, “Describing small-scale structure in random media using pulse-echo ultrasound”, *J. Acoust. Soc. Am.* **87**(1), 179-192, 1990.
- [6] E. J. Feleppa, T. Liu, A. Kalisz, M. C. Shao, N. Fleshner, V. Reuter and W. R. Fair, “Ultrasonic spectral-parameter imaging of the prostate”, *Int. J. Imaging Syst. Technol.* **8**(1), 11-25, 1997.
- [7] M. L. Oelze, W. D. O’Brien Jr., J. P. Blue and J. F. Zachary, “Differentiation and characterization of rat mammary fibroadenomas and 4T1 mouse carcinomas using quantitative ultrasound imaging”, *IEEE Trans. Med. Imaging*, **23**(6), 764-771, 2004.

- [8] R. M. Vlad, N. M. Alajez, A. Giles, M. C. Kolios and G. J. Czarnota, "Quantitative ultrasound characterization of cancer radiotherapy effects *in vitro*", *Int. J. Radiat. Oncology Biol. Phys.*, **72**(4), 1236-1243, 2008.
- [9] K. K. Shung and G. A. Thieme, "Ultrasound scattering in biological tissues", CRC Press, Boca Raton, 1993.
- [10] R. B. Ami, G. Barshtein, D. Zeltser, Y. Goldberg, I. Shapira, A. Roth, G. Keren, H. Miller, V. Prochorov, A. Eldor, S. Berliner and S. Yedgar, "Parameters of red blood cell aggregation as correlates of the inflammatory state", *American Journal of Physiology (Heart & Circulatory Physiology)*, vol. 280(5), pp. H1982-H1988, 2001.
- [11] F. T. H. Yu and G. Cloutier, "Experimental ultrasound characterization of red blood cell aggregation using the structure factor size estimator", *J. Acoust. Soc. Am.* **122**(1), 645-656, 2007.
- [12] F. T. H. Yu, E. Franceschini, B. Chayer, J. K. Armstrong, H. J. Meiselman, G. Cloutier, "Ultrasonic parametric imaging of erythrocyte aggregation using the structure factor size estimator", *Biorheology*, **46**(4):343-363, 2009.
- [13] E. Franceschini, F. T. H. Yu, F. Destrepes and G. Cloutier, "Ultrasound characterization of red blood cell aggregation with intervening attenuating tissue-mimicking phantoms", *J. Acoust. Soc. Am.* **127**(2), 1104-1115, 2010.
- [14] [http://en.wikipedia.org/wiki/Close-packing\\_of\\_spheres](http://en.wikipedia.org/wiki/Close-packing_of_spheres)
- [15] D. Savéry and G. Cloutier, "High-frequency ultrasound backscattering by blood: Analytical and semi-analytical models of the erythrocyte cross-section", *J. Acoust. Soc. Am.*, 121(6): 3963-3971, 2007.

- [16] P. M. Morse and K. U. Ingard, "Theoretical acoustics", Princeton University Press, Princeton, NJ, 1968, Chapter 8.
- [17] K. K. Shung, Y. W. Yuan, D. Y. Fei and J. M. Tarbell, "Effect of flow disturbance on ultrasonic backscatter from blood", *J. Acoust. Soc. Am.* **75**(4), 1265-1272, 1984.
- [18] R. K. Saha and G. Cloutier, "Monte Carlo study on ultrasound backscattering by three-dimensional distributions of red blood cells", *Physical Review E*, **78**, 061919, 2008.
- [19] D. Savéry and G. Cloutier, "Effect of red cell clustering and anisotropy on ultrasound blood backscatter: A Monte Carlo study", *IEEE Trans. Ultrason. Ferroelectr. Freq. Control*, **52**(1), 94-103, 2005.
- [20] E. L. Hinrichsen, J. Feder and T. Jøssang, "Random packing of disks in two dimensions", *Physical Review A*, **41**(8), 4199-4209, 1990.
- [21] J. G. Berryman, "Random close packing of hard spheres and disks", *Physical Review A*, **27**(2), 1053-1061, 1983.
- [22] W. S. Jodrey and E. M. Tory, "Computer simulation of close random packing of equal spheres", *Physical Review A*, **32**(4), 2347-2351, 1985.
- [23] R. K. Saha, S. K. Sharma and M. C. Kolios, "Single cell size estimation from backscattered spectrum by using some weak scattering approximations", *Canadian Acoustics*, **38**(2), 31-34, 2010.
- [24] B. G. Teh and G. Cloutier, "Modeling and analysis of ultrasound backscattering by spherical aggregates and rouleaux of red blood cells", *IEEE Trans. Ultrason. Ferroelectr. Freq. Control*, **47**(4), 1025-1035, 2000.

- [25] Y. W. Yuan and K. K. Shung, "Ultrasonic backscatter from flowing whole blood. II: Dependence on frequency and fibrinogen concentration", *J. Acoust. Soc. Am.* **84**(4), 1195-1200, 1988.
- [26] R. M. Vlad, R. K. Saha, N. M. Alajez, S. Ranieri, G. J. Czarnota and M. C. Kolios, "An increase in cellular size variance contributes to the increase in the ultrasound backscatter during cell death", *Ultrasound Med. Biol.* **36**(9), 1546-1558, 2010.

## Figure captions:

Figure 1. Flow chart illustrating simulation steps to generate spherical clusters with hexagonal close packing (HCP) of red blood cells.

Figure 2. (a) An arrangement of 51 spheres (representing RBCs) in hexagonal close packing configuration forming a RBC cluster. (b) It shows a simulated aggregated blood tissue sample containing 4 clusters where each cluster is composed of 51 spheres. The non-overlapping clusters are randomly placed in the ROI under periodic boundary conditions. For clarity, a smaller ROI at a lower hematocrit ( $H \approx 14\%$ ) is shown.

Figure 3. (Color online). (a) Variations of the backscattering coefficient with interrogating frequency at different simulated mean cluster sizes for  $H = 0.20$ . The black line corresponds to BSC predicted by the Percus-Yevick packing theory. (b) Same as (a) but for  $H = 0.30$ . (c) Same as (a) but for  $H = 0.40$ . (d) Increase of BSC with respect to that of the Percus-Yevick packing theory in dB with cluster size at 7.5 MHz. Variations at three hematocrits are shown.

Figure 4. (Color online). (a) BSC curves fitted with the SFSE model at different clustering conditions at  $H = 0.20$ . Both  $R_{sp}$  and  $W$  estimated by the SFSE method are given in the legend. (b) Same as (a) but for  $H = 0.30$ . (c) Same as (a) but for  $H = 0.40$ .

Figure 5. (Color online). (a) Comparison of estimated aggregate size with actual aggregate size at three hematocrits ( $H = 0.20, 0.30$  and  $0.40$ ). (b) Plot of  $W$  as a function of square of the actual aggregate size at different hematocrits.

Figure 6. (Color online). Illustration of changes in spectral slope for a simulated BSC curve.

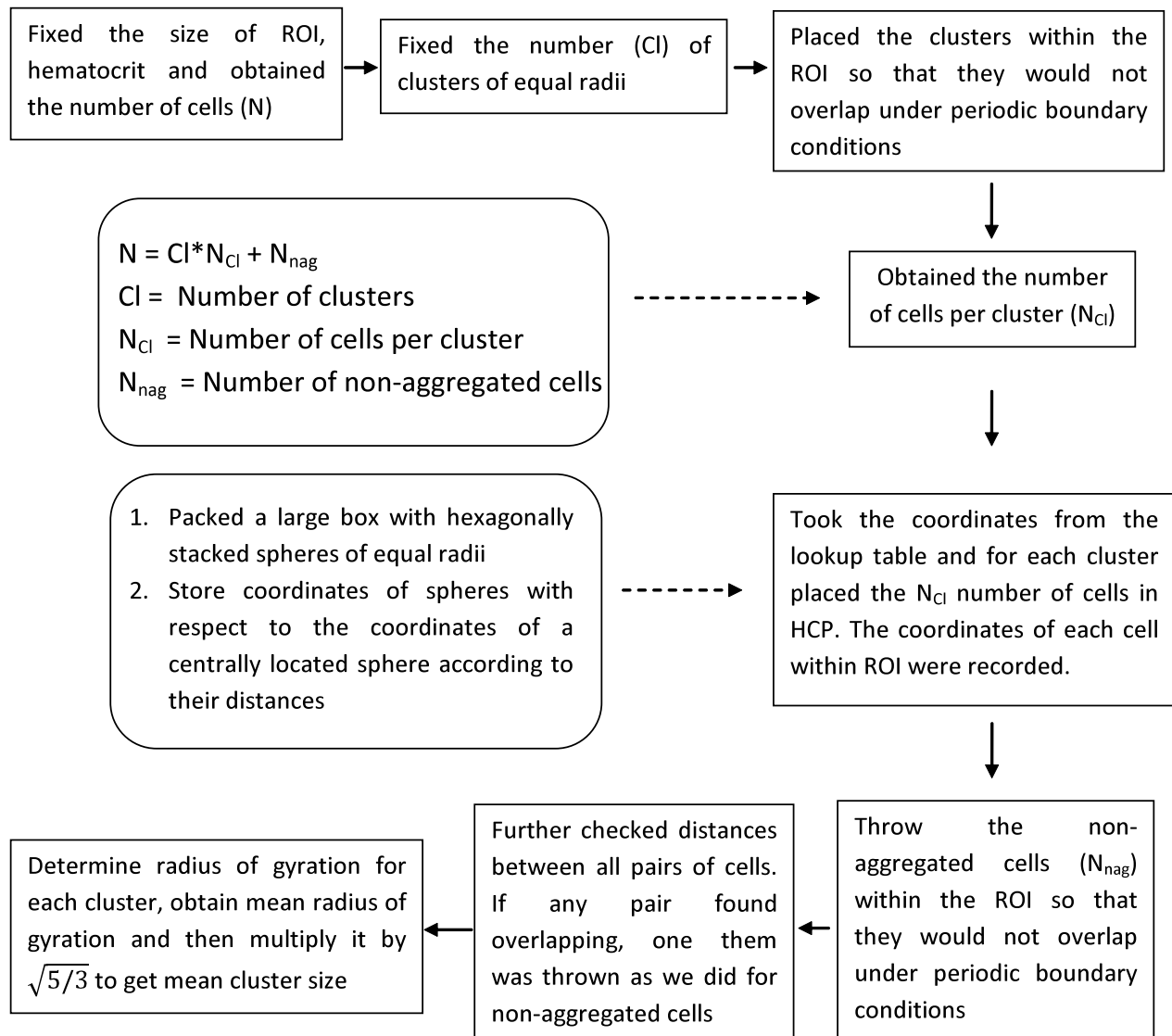


Figure 1.

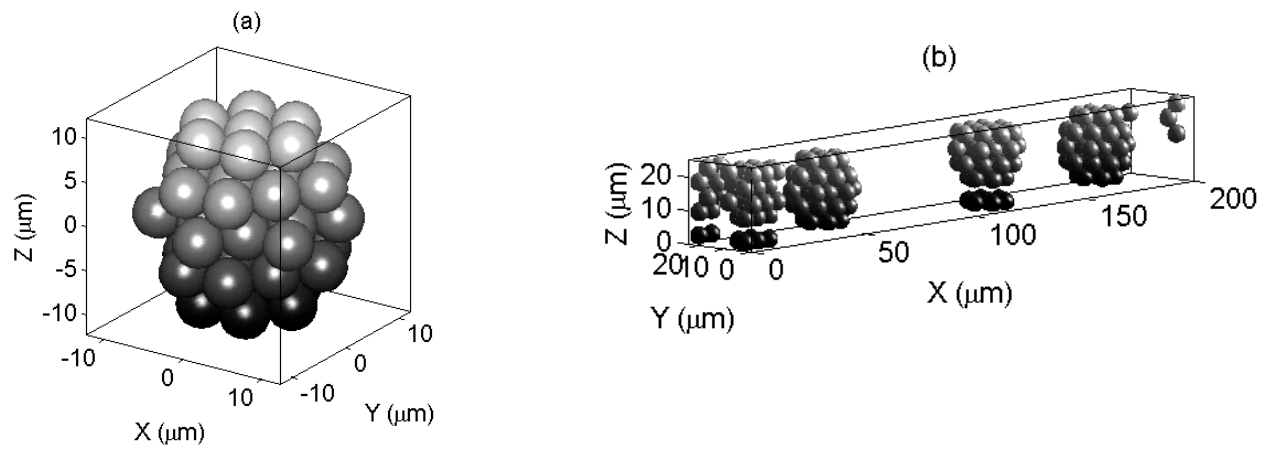


Figure 2.

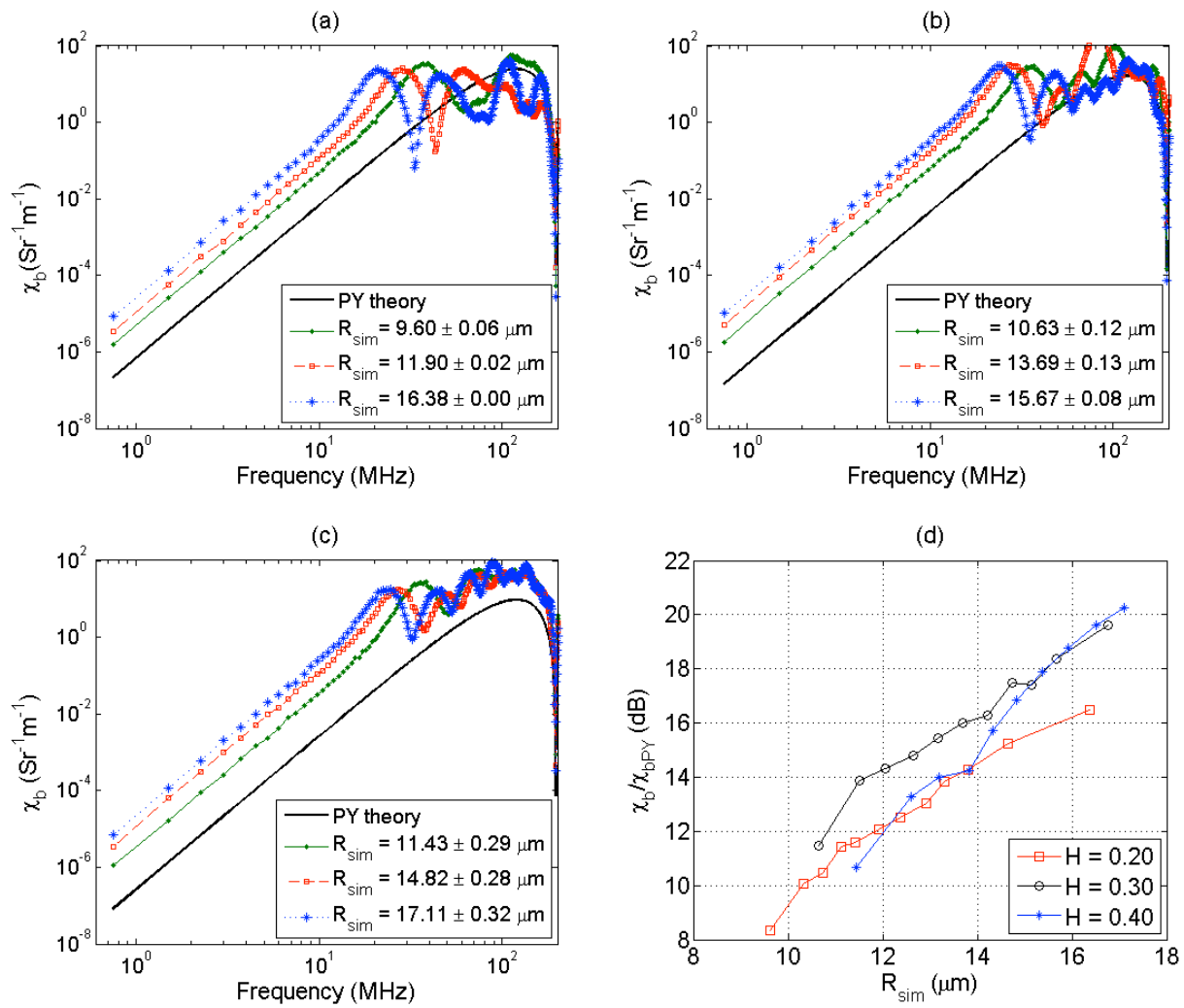


Figure 3.

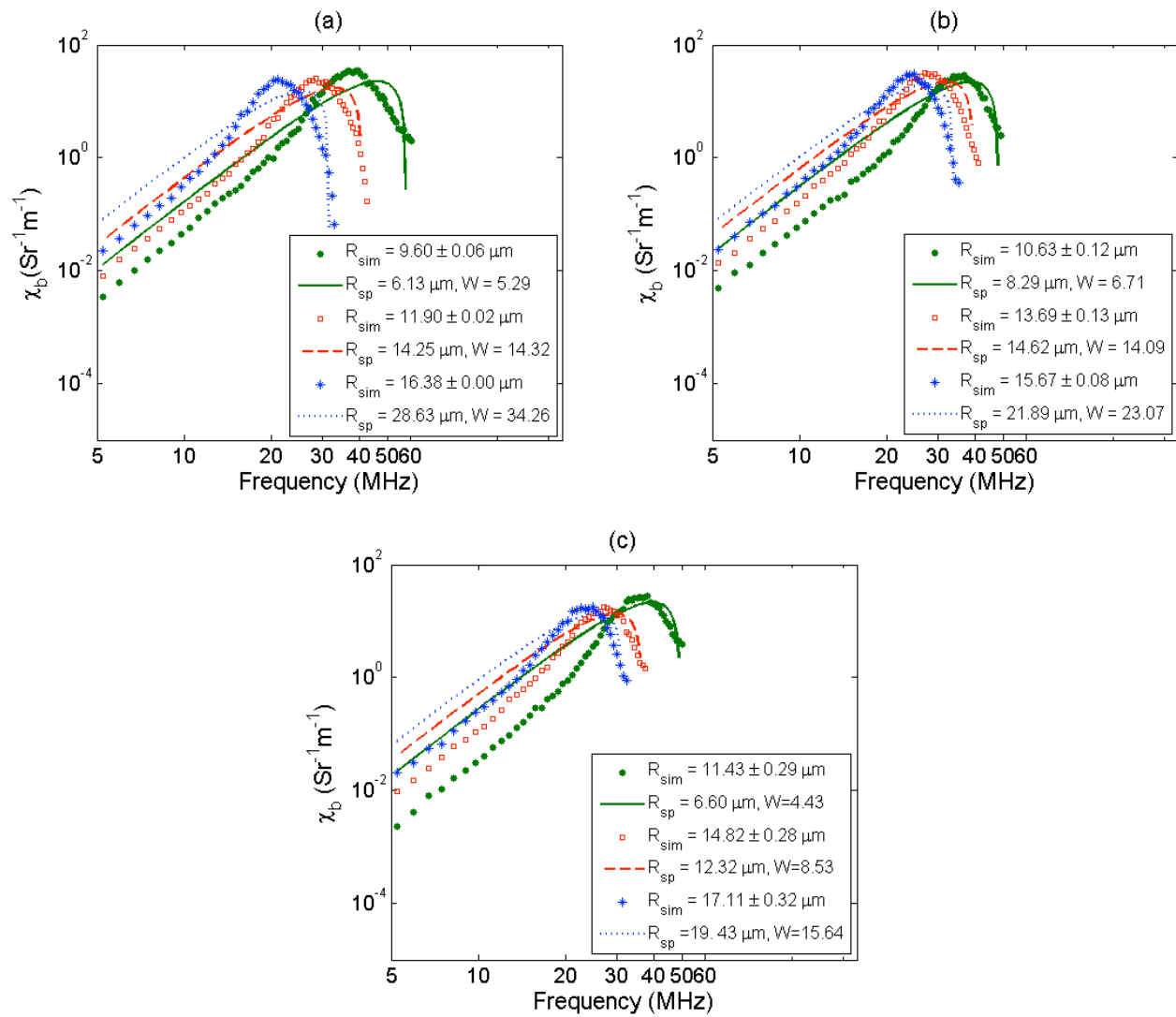


Figure 4.

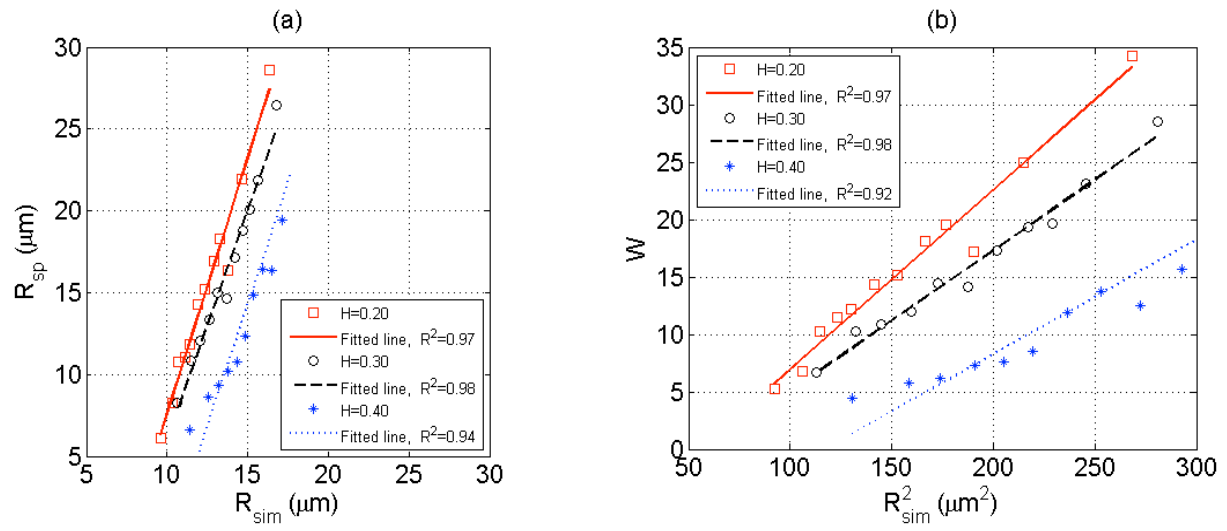


Figure 5.

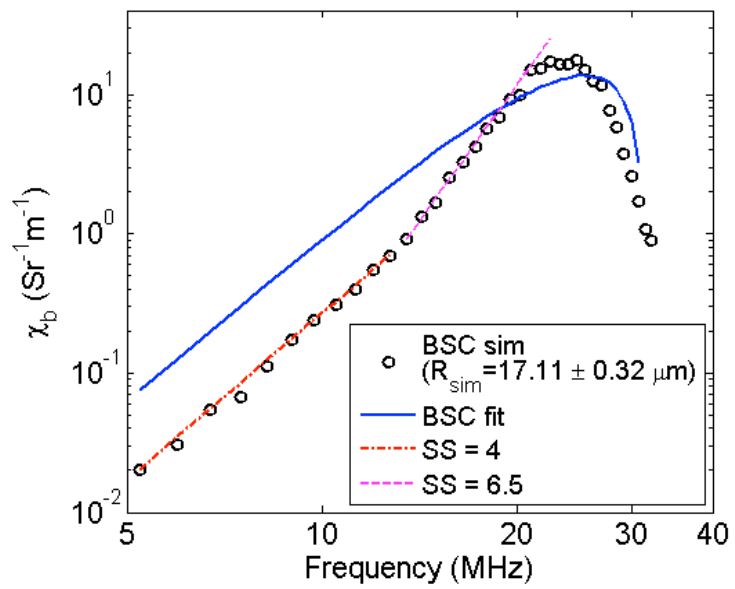


Figure 6.